Vol. 5 No. 2 (2026)

Pakistan Journal of Medical & Cardiological Review

https://pakjmcr.com/index.php/1/about

Online ISSN 3007-2387

Print ISSN 3007-2379

Explainable Deep Learning for Brain Cancer Classification: A Comparative Study of Transfer Learning and Training-from-Scratch Models Using SHAP and LIME

Asif Rahman
Department of Computer Science, Abdul Wali Khan University, Mardan, KPK, Pakistan. Email: asifrahman557@gmail.com

Maqsood Hayat
Department of Computer Science, Abdul Wali Khan University, Mardan, KPK, Pakistan. Email: m.hayat@awkum.edu.pk

Nadeem Iqbal
Department of Computer Science, Abdul Wali Khan University, Mardan, KPK, Pakistan. Email: nikhan@awkum.edu.pk

Hashim Ali
Department of Computer Science, Abdul Wali Khan University, Mardan, KPK, Pakistan. Email: hashimali@awkum.edu.pk

Ishaq Ahmad
Department of Computer Science& Information Technology, University of Malakand, KPK, Pakistan. Email: ishaqictm@gmail.com

Author Details

Keywords: Brain Tumor Detection; MRI; CNN; Transfer Learning; VGG16; LIME; SHAP

Received on 6 Mar 2026
Accepted on 8 Apr 2026
Published on 14 Apr 2026

Corresponding E-mail & Author*:

Asif Rahman
Department of Computer Science, Abdul Wali Khan University, Mardan, KPK, Pakistan. Email: asifrahman557@gmail.com

Abstract

Diagnosing brain cancer with Magnetic Resonance Imaging (MRI) is not only critical but also a very difficult and time-consuming task in medical analysis of images. Despite the Deep Learning (DL) model's performance with interpretability, the DL still dramatically enhances the ability to automate the procedure. In this research study, we first trained a convolutional neural network (CNN) from scratch on 2,000 MRI images, comprising 1,000 tumors and 1,000 non-tumors, and then tested it on 600 images, comprising 300 tumors and 300 non-tumors. The scratch model (CNN) achieved 98% accuracy with sensitivity 100%, precision 96%, F1-score 98%, and specificity 96%. To enhance performance, we proceeded to transfer learning using four models: DenseNet121, InceptionV3, ResNet50, and VGG16. Among these architectures, VGG16 achieved the best results, achieving perfect classification across all evaluation metrics (e.g., accuracy, precision, sensitivity, F1-score, and specificity: 100%). To discuss the challenges in interpretability, we also applied model explainability techniques to visualize the result-making procedures of VGG16, e.g., Shapley Additive Explanations (SHAP) and Local Interpretable Model-agnostic Explanations (LIME). Both local and global insights from these explainability methods were provided, highlighting critical tumor regions, validating the model's predictions, and enhancing trust in its real-world clinical applications. The results

confirmed that VGG16 achieved the highest performance and provided interpretable explanations, making it a robust and trustworthy model for automating the brain cancer diagnosis process. asifrahman557/Explainable-AI-using-SHAP-LIME

1. Introduction

The most important functions of the human body, such as decision-making, coordination, and communication, are performed by the central nervous system (CNS). The CNS has mainly two parts: the brain and the other is the spinal cord [1, 2]. As the structure of this body part is extremely complex, that is why it is more vulnerable to various kinds of disorders like stroke, infections, headaches, and particularly brain tumors, which is among the most critical situations to detect and deal effectively [3]. There are benign and malignant tumors, with more than 200 neoplasm subtypes recognized in medical literature[4]. In the human body, the abnormal enhancement of brain cells is actually a brain tumor, but even a minor growth can also disturb neurological function, posing life-threatening dangers [5-9]. Brain tumors have become a major global health challenge, which is actually formed by the abnormal growth of tissue in the brain. Among the ten leading causes of death in children and adults, the Brain cancer ranks among them [10], with varying survival rates which greatly depend on tumor type, the location in the CNS, and severity [11-13]. Four million people fight brain cancer, and more than 1.2 million die [14]. A huge figure of 300% growth in brain cancer deaths in the past three decades was stated in the report of the National Brain Tumor Foundation (NBTF) [15], pinpointing the eagerness for timely diagnosing and precise categorization [16, 17]. National Brain Tumor Foundation (NBTF) also reported that demise ratio have tripled in the middle- as well as low-income lands [18]. Specific and early diagnosis is extremely important, as the growth of brain cancer could be fast, which can severely affect patient survival [19]. As the physical monitoring of MRI brain scans is lengthy and labor-intensive, it also requires a number of experts and is prone to obvious human errors, emphasizing the requirement for an automated diagnostic system [20].

MRI is a non-invasive and widely used tool for brain cancer detection [21, 22]. Each year, Millions of MRI scans are conducted, but only a few detect malignancy [23]. In adults and children, a steady rise in brain cancer has been recorded by the global cancer statistics [24-26]. Accurate diagnosis of brain cancer is persistently difficult due to the size variability, structures, and locations. Biopsies and gamma knife (traditional procedures) are lengthy, frustrating, and time-consuming, underscoring the importance of MRI as an ideal tool. ML techniques can analyze large datasets, reduce redundancy, and improve diagnostic results by focusing on the most pertinent characteristics [27]. Feature selection techniques (FSTs), such as Linear Discriminant Analysis (LDA), Principal Component Analysis (PCA), and Mutual Information (MI), play a significant role in dataset filtering, improving classification accuracy, and reducing computational complexity [28].

Brain cancer detection has been enhanced by recent advancements in computational intelligence. Due to their superior performance compared with traditional techniques, ML and DL methods have been widely adopted. Almadhoun et al. [29] attained 98% test accuracy on 10,000 MRI scans using DL approaches, while Musallam et al. [30] conveyed 97.72% accuracy with a DCNN in four tumor subtypes. Correspondingly, EfficientNet [31] and residual CNNs [32] attained accuracies above 97%, whereas Khalil et al. [33] employed an improved Dragonfly algorithm for tumor detection with 98.2% accuracy. Strong results have also been demonstrated by Hybrid CNN models, as shown by Sajid et al. [34] gaining 91% specificity. DL algorithms, which are a subset of ML, have expanded approval for processing medical images like MRI brain scans and are broadly functional in cancer diagnosing, including lung [35], gastroscopy biopsy [36], and brain tumors [37-40]. To precisely spot tumor-affected scans, a large MRI dataset was proficiently processed with DL models [14].

In the medical domain, the MRI remains the most common imaging modality. Research studies using CNNs have revealed strong performance: Abiwinanda [41] attained 98.51% training accuracy on 3064 T1-weighted MRI brain scans, and Rehman et al. [42] found that VGG16 outclassed AlexNet and GoogLeNet with 98.69% accuracy. Pashaei et al. [41] confirmed CNN dominance over MLP, XGBoost, and SVM, while Paul et al. [43] completed 91.43% accuracy by means of fully connected networks. Ensemble classifiers have also been discovered, with Garg et al. [19] giving 97.3% accuracy. Noreen et al. [44] presented a manifold feature extraction technique, while K-means clustering was used for tumor segmentation, for early finding [45, 46]. Deep neural networks have also been used for the purpose of brain tumor examination [47]. Amin et al. [19] proposed an AI model achieving 96.08% accuracy on 1321 MRI scans from 153 patients. Rehman et al. [48] established a Brain Tumor Localization strategy through Gabor filters, which exposed restrictions in accurate detection.

Traditional techniques of ML originally depended on hand-crafted features [49], but the after-research studies exposed CNNs with optimization methods such as PSO [50, 51] can increase segmentation accuracy more than 92%. CNN-based architectures, including 3D-VGGNet and 3D-ResNet, described accuracies close to 80% for Alzheimer's and tumor classification processes [52], whereas models like ResNet-50 touched 96.5% in tumor diagnosis [53].

New hybrid and multimodal methods have also developed. VGGNet-SVM groupings reached 96% accuracy [54], while CNNs with genetic algorithms improved glioblastoma recognition [55]. Classification performance additionally upgraded image preprocessing and enhancement [56]. Segmentation-focused networks such as "DeepMedic" and BraTS-based ML models verified good performance on standard datasets [57, 58]. The hybrid techniques merging ML classifiers and DL-extracted features have been thoroughly studied, yet they are often computationally expensive [59]. Younis et al. [60] conveyed 98.15% accuracy using VGG-16 and 98.41% with ensemble models, while Zahid et al. [61] accomplished 94.4% accuracy with ResNet101. A 3D deep neural network reached Dice scores of 0.81, 0.69, and 0.55 [62] for the BRATS datasets, while Sharif et al. [63][36] reported accuracies above 98% on BRATS2018 and BRATS2019.

DL and ML techniques are increasingly applied in medical imaging with the rapid advances in artificial intelligence (AI). Exceptional success in image classification [64-67], medical diagnosis [68-70], and tissue segmentation [71-73] was demonstrated by Convolutional Neural Networks (CNNs). In medical imaging, CNNs outperform conventional methods, acquiring state-of-the-art detection accuracy [74-76]. Supervised learning methods are generally effective for brain cancer categorization, in which labeled MRI datasets distinguish tumor from non-tumor scans [77-81]. Previous research has evaluated ML models such as Random Forests (RF), Support Vector Machines (SVM), and k-Nearest Neighbors (KNN) for medical analysis, but often with an imperfect examination of feature selection strategies [82-84]. Most of the preceding studies have identified numerous DL models for brain tumor diagnosis [21, 85-91], but many of them lack complete judgements using traditional ML techniques, or they need more complex computations [42, 43, 92, 93].

Therefore, this research study reports the grave need for precise and explainable brain cancer categorization models by analytically comparing CNNs trained from scratch with transfer-learning architectures, e.g., DenseNet121, InceptionV3, ResNet50, and VGG16. Our results validate that VGG16 not only achieves superior accuracy and the best results across all evaluation metrics but also, when combined with explainable AI methods, e.g., LIME and SHAP, delivers transparent, explainable predictions. This combination of high-performance DL with explainability confirms that the models are not only technically robust but also appropriate for potential clinical implementation, which supports radiologists and other healthcare professionals in making more informed and consistent problem-solving decisions.

2. Materials and Methods

2.1.Dataset Acquisition

For this research, a dataset of brain MRI scans was obtained from Kaggle, which included both tumor and non-tumor instances. A sub-total of 2,600 MRI scans was acquired and used. This group of images was distributed as 2,000 images, with 1,000 tumors and 1,000 non-tumors for training; however, 600 images, with 300 tumors and 300 non-tumors, were used for testing. This dataset was preprocessed to ensure homogeneous image scope and quality, facilitating consistent performance throughout model training.

2.2. Data Preprocessing

To match the CNN architectures' requirements, all MRI brain scans were resized to 224 × 224 pixels. Additionally, pixel intensity standardization was performed to ensure the values fell within the [0, 1] range, which improved convergence during training. Various data expansion methods, such as spinning, overturning, and enhancement, were applied to the training dataset to improve model generalization and avoid overfitting.

2.3.Experimental Setup

This research aimed to assess the DL model's performance for brain cancer detection and categorization by comparing the learning from scratch and transfer learning methods.

2.4.CNN Learning from Scratch

The CNN architecture was trained from scratch using the training dataset. This architecture consisted of many convolutional and pooling layers.

2.5.Transfer Learning Models

To power the knowledge from models, earlier trained on large image datasets, pre-trained architectures were utilized through transfer learning. These models included:

- DenseNet121
- InceptionV3
- ResNet50
- VGG16

The top layers of each model were replaced with fully associated layers tailored for binary classification. The transfer learning method was guided by pre-trained weights on the MRI brain scan dataset, with dropout layers incorporated to mitigate overfitting.

3. Model Evaluation

Accuracy, sensitivity, specificity, precision, and F1 Score were used to assess the model's performance. These metrics are the most important for delivering a comprehensive valuation of a model's ability.

3.1.Explainable AI Analysis

VGG16 achieved superior performance across all evaluation metrics, which is why this model was examined using explainable AI-based methods to fully understand its decision-making process. LIME and SHAP were used to provide visual descriptions of the parts/sections of the MRI scans that substantially influenced the model's decision. For clinical implementations, the model analysis not only provided interpretability but also increased confidence.

3.2.Implementation Details

Python 3.9 with TensorFlow 2.12 and Keras API were used in these experiments. All visualizations of LIME and SHAP explanations were generated using their respective

Python libraries, producing interpretable heatmaps for qualitative examination.

3.3.Enhanced Materials and Methods with Workflow Diagram

Figure 1 summarizes the overall methodology of this research, illustrating the step-by-step procedure from dataset collection to the examination of explainable AI.

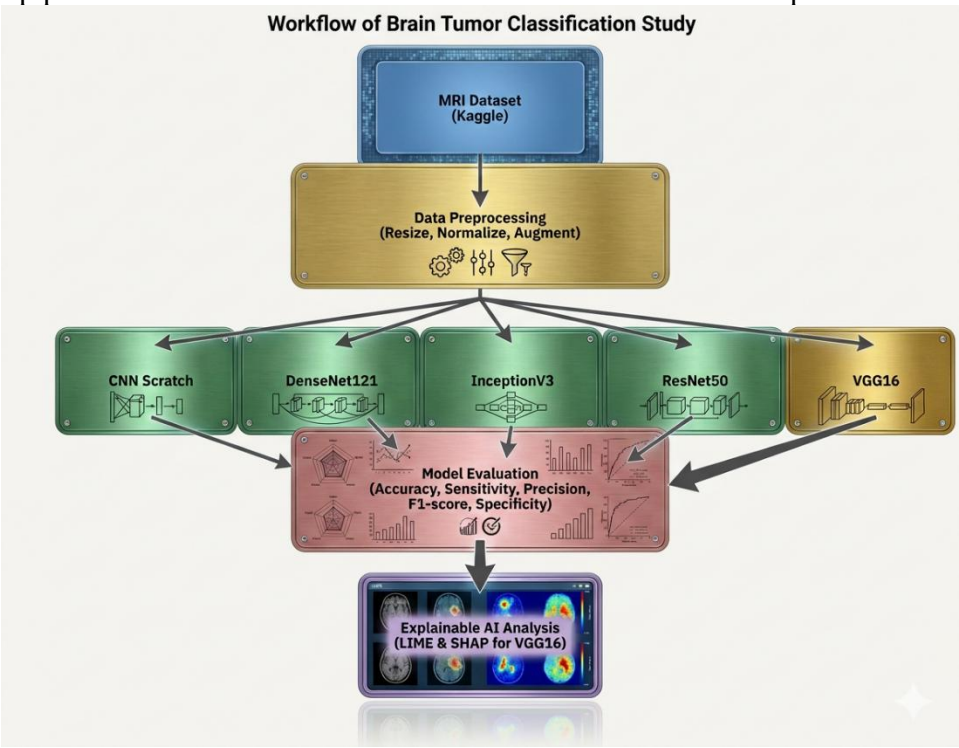

Figure 1: Workflow of Brain Tumor Classification of this study

4. Classification Models

In this research, we utilized both the learning-from-scratch and transfer-learning approaches to categorize brain scans into tumor and non-tumor classes. Models used are CNN trained from scratch and four pre-trained models: DenseNet121, InceptionV3, ResNet50, and VGG16. These models are shortly described below.

4.1.CNN Learning from Scratch

CNNs are commonly used for MRI classification because they automatically absorb spatial hierarchies of features. A CNN typically contains convolutional, pooling, and fully connected layers.

Convolution Operation: For an input image (I) and a filter (K), this operation can be mathematically expressed in an equation 1, as:

$$S(i,j) = (I * K)(i,j) = \sum_{m} \sum_{n} I(i-m, j-n)\ .\ K(m,n) \qquad \text{Equation 1}$$

Where:

$\boldsymbol{I(i-m, j-n)}$: Represents the Input Image or the feature map from a previous layer. The indices (i, j) track the current position of the filter on the image.

$\boldsymbol{K(m,n)}$: Represents the Kernel or Filter. It is a small matrix of learnable weights designed to detect specific patterns, such as edges, textures, or tumor boundaries.

*: Represents the convolution mathematical operator performed on the image.

$\boldsymbol{S(i,j)}$**:** Represents the Feature Map (Output). It highlights where the specific features defined by the filter **K** were found in the image **I**.

ReLU as an activation function: This function is applied immediately after the convolution. It keeps positive values (important features) and turns all negative values to zero (noise), refining the feature map $\boldsymbol{S(i,j)}$ before it moves to Model

Evaluation**.** The ReLU function is written in equation 2.

$f(x) = \max(0, x)$ $Equation\ 2$

Pooling Layer: To reduce computational complexity and extract dominant features from brain MRI scans, a Max Pooling layer is applied after the activation phase. Which performs a down-sampling operation by selecting the maximum value within a specified local neighborhood (window). The Max Pooling equation is written in equation 3.

$$\gamma_{i,j} = \max_{(m,n)\in\omega indow} x_{i+m,j+n} \quad \text{Equation 3}$$

Where:

$\boldsymbol{x_{i+m,j+n}}$**:** Represents the pixel value (activation) within the local window of the input feature map.

$\boldsymbol{\gamma_{i,j}}$: Represents the resulting value in the reduced output feature map.

$\boldsymbol{\omega\dot{i}ndow}$: Defines the spatial neighborhood (e.g.,2 X 2) over which the maximum operation is computed.

4.2.DenseNet121 Transfer Learning

Dense connectivity represents a fundamental shift in how information flows through a neural network. Unlike traditional architectures, in which each layer connects only to its immediate successor, dense connectivity creates a more collaborative learning environment in which every layer receives direct input from all preceding layers. This elegant concept is captured mathematically in Equation 4.

$$\$X\_l = H\_l([X\_0, X\_1, \ldots\ldots, X\_\{l-1\}])\$ \quad \text{Equation 4}$$

Where:

$\$\boldsymbol{X\_l}$: represents the output of the current layer.

$\$\boldsymbol{H\_l}\$$: denotes the transformation function applied at this layer. The input to this function is the concatenation of feature maps from every previous layer - from the initial input ***X_0*** all the way through ***X_{l-1}.*** This means that each layer has direct access to the raw features and all the refined representations developed earlier in the network.

4.3.InceptionV3 Transfer Learning

This model is based on the Inception module, which uses parallel convolutional filters of diverse sizes. The output of the inception module is represented in equation 5.

$$y = Concat\ [f_{1*1}(x), f_{3*3}(x), f_{5*5}(x), Pool(x)] \quad \text{Equation 5}$$

Here**, f_{n* n}** represents a convolutional operation with an **$n * n$** filter. The **1 * 1** convolutions capture pointwise features and help manage dimensionality, while the **3 * 3** and **5 * 5** filters progressively capture increasingly broader spatial patterns. The parallel pooling operation preserves essential spatial information while adding another layer of feature extraction.

4.4.ResNet50 Transfer Learning

ResNet50 utilizes residual connections to train very deep networks easily. This concept is formalized in the residual learning formula shown in Equation 6.

$$Y_l = F(X_l, W_l) + X_l \quad \text{Equation 6}$$

Where:

$\boldsymbol{X_l}$ represents the input to a residual block, while $\boldsymbol{F(X_l, W_l)}$ denotes the residual mapping to be learned—essentially, the transformation that captures what needs to be added to the input. The output $\boldsymbol{Y_l}$ is obtained by simply adding the original input to this learned residual.

4.5.VGG16 Transfer Learning

A deep CNN with 16 weight layers is VGG16. It is known for its ease and even architecture using 3×3 convolutional filters. In a convolutional layer, the network

applies a filter (kernel) to the input feature map to extract spatial patterns such as edges, textures, and shapes. Each filter slides across the input image, performing an element-wise multiplication followed by a summation to produce a feature map.

The convolution operation can be expressed as:

$$y_{i,j}^{(k)} = \sum_{m=0}^{2} \sum_{n=0}^{2} x_{i+m,j+n} \cdot w_{m,n}^{(k)} + b^{(k)} \qquad \text{Equation 7}$$

where:

$\boldsymbol{x_{i+m,j+n}}$: Represents the input pixel value within the receptive field.

$\boldsymbol{w_{m,n}^{(k)}}$: Denotes the weight of the $\boldsymbol{k^{th}}$convolution filter.

$\boldsymbol{b^{(k)}}$**:** Represents the bias term associated with the filter.

$\boldsymbol{y_{i,j}^{(k)}}$ **:** Represents the resulting output feature map value at location $(\boldsymbol{i, j})$

Table 1 provides a comprehensive overview of the models utilized in this study.

Table 1: Summary of Model Properties

Model	Depth	Key Feature	Advantage
CNN Scratch	Custom	Learned from MRI dataset	Flexible, dataset-specific
DenseNet121	121	Dense connectivity	Feature reuse, gradient flow improvement
InceptionV3	48	Multi-scale convolutions	Captures multi-scale features
ResNet50	50	Residual connections	Solves vanishing gradient, deep learning
VGG16	16	Uniform 3×3 convolutions	Simple, effective, interpretable

5. Quantitative Performance Valuation Metrics

The five standard performance metrics were calculated to examine the efficiency of brain cancer classification models: Accuracy, Sensitivity, Specificity, Precision, and F1 Score.

5.1.Accuracy

$$Accuracy = \frac{Number\ of\ Correct\ Predictions\ (NCP)}{Total\ Number\ of\ Predictions\ (TNP)} \qquad \text{Equation 8}$$

where:

Number of Correct Predictions (NCP) is the total number of instances correctly classified by the model.

Total Number of Predictions (TNP) represents the overall number of samples evaluated by the model.

5.2.Sensitivity (Recall)

$$Sensitivity = \frac{True\ Positives\ (TP)}{TP + False\ Negatives\ (FN)} \qquad \text{Equation 9}$$

where:

True Positives (TP) are the number of positive instances correctly identified by the model.

False Negatives (FN) represent the number of positive instances that the model

incorrectly classifies as negative.

5.3.Specificity

$$Specificity = \frac{True\ Negatives\ (TN)}{TN + False\ Positives\ (FP)} \qquad Equation\ 10$$

where:

True Negatives (TN) are the number of negative instances correctly classified by the model.

False Positives (FP) are the number of negative instances incorrectly classified as positive.

5.4.Precision

$$Precision = \frac{True\ Positives\ (TP)}{TP + False\ Positives\ (FP)} \qquad Equation\ 11$$

where:

True Positives (TP) are the number of positive instances correctly identified by the model.

False Positives (FP) are the number of negative instances incorrectly classified as positive.

5.5.F1 Score

$$F1\ Score = 2.\frac{Precision\ .Sensitivity}{Precision + Sensitivity} \qquad Equation\ 12$$

where:

Precision measures the proportion of correctly predicted positive instances among all predicted positive instances.

Sensitivity (Recall) measures the proportion of actual positive instances that are correctly identified by the model.

6. The Deep Learning Models

Table 2 below presents a brief overview of several DL models applied to brain cancer categorization. The models assessed, shown in Table 1, include a CNN trained from scratch and pre-trained transfer-learning architectures: DenseNet121, InceptionV3, ResNet50, and VGG16. Every model was assessed using metrics, namely Accuracy, Sensitivity, Precision, F1 Score, and Specificity, to deliver a complete assessment of their classification abilities.

All the DL models reached high overall accuracy, with CNN, DenseNet121, and InceptionV3 feat 98%, and VGG16 attaining a perfect 100%. Sensitivity and precision metrics indicate that VGG16 accurately recognized all tumor and healthy cases, outperforming the other DL models. On the other hand, ResNet50, while reaching comparable overall accuracy, presented lower sensitivity (86%) and precision (80%). Generally, the outcomes indicated that VGG16 Transfer Learning delivers better performance across all metrics and demonstrates robust, balanced classification, making it the most appropriate model for further explainable AI assessment.

Table 2: The Deep Learning Models

Model	Accuracy (%)	Sensitivity (%)	Precision (%)	F1 Score (%)	Specificity (%)
CNN Learning from Scratch	98	100	96	98	96
Dense Net121	98	99	97	98	97

Transfer Learning					
InceptionV3 Transfer Learning	98	98	98	98	98
ResNet50 Transfer Learning	98	86	80	83	79
VGG16 Transfer Learning	100	100	100	100	100

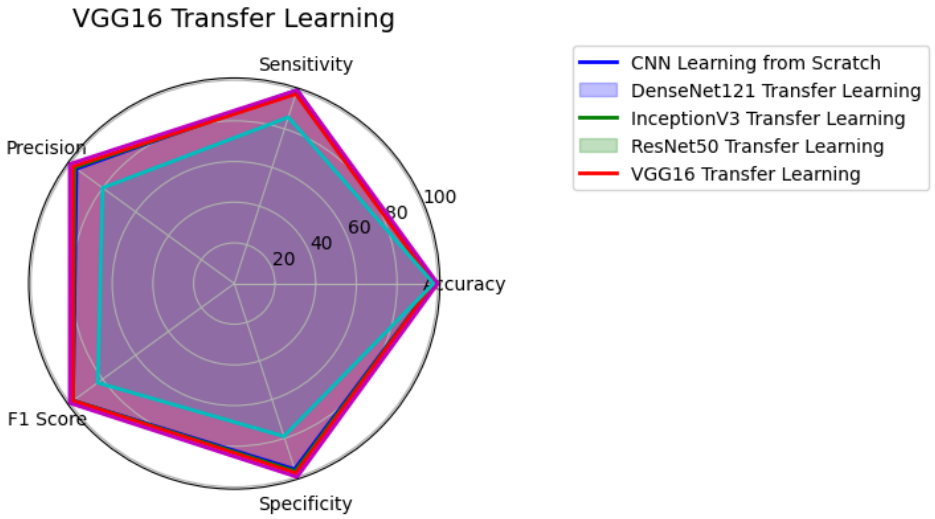

Figure 2: VGG16 Transfer Learning Spider Chart

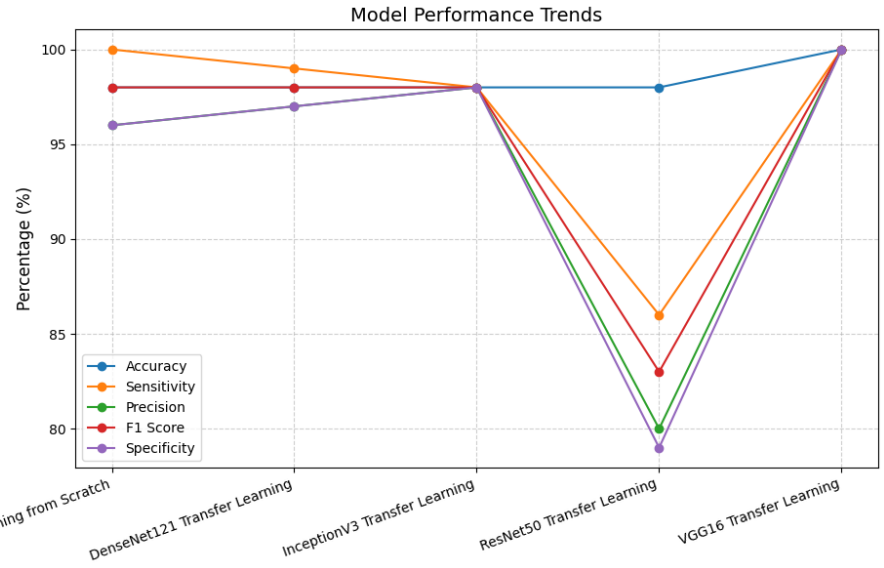

Figure 3: VGG16 Transfer Learning Line graph

The graphic representations in Figures 2 and 3 show that the performance metrics provide a strong pictorial comparison of the five DL models. From the above figures, it is clear that VGG16 consistently outperforms all other models, achieving perfect scores in Accuracy, Sensitivity, Precision, F1 Score, and Specificity. The CNN trained from scratch, as well as InceptionV3, also validate strong overall performance; however, subtle alterations are noticeable in their sensitivity and precision results. It was observed that ResNet50, though preserving high overall accuracy, exhibits lower

sensitivity and precision, indicating a higher rate of misclassifying tumor cases compared with the other DL models. DenseNet121 displays improved balance among sensitivity and specificity. Overall, the visual assessment fortifies the numerical results, which confirmed that VGG16 delivers the best performance. They made us the perfect choice for explainable AI-based examination through LIME and SHAP.

6.1.Analysis of Learning from Scratch and Transfer Learning Models

This research assessed the performance of DL architectures, e.g., CNNs (trained from scratch) and transfer-learning models (e.g., DenseNet121, InceptionV3, ResNet50, VGG16). The objective was to classify brain MRI scans for tumors. These models were evaluated using metrics (e.g., accuracy, sensitivity, precision, F1-score, specificity) to gain a comprehensive understanding of their classification performance.

6.2.CNN (Learning from Scratch)

The CNN recorded 98% accuracy, 100% sensitivity, and 96% precision. The results show that this model identified all tumor images without missing any, which is an extremely important characteristic in medical image diagnosis. However, its somewhat inferior precision relative to VGG16 suggests the occurrence of some false positives. The specificity of 96% further supports the conclusion that, while the CNN performed well at detecting non-tumor images, there was still room to improve false-positive rates. However, reaching such high performance without pre-trained weights imitates the strength of the custom architecture in learning discriminative features directly from the dataset. These results are illustrated in Figure 4 as follows:

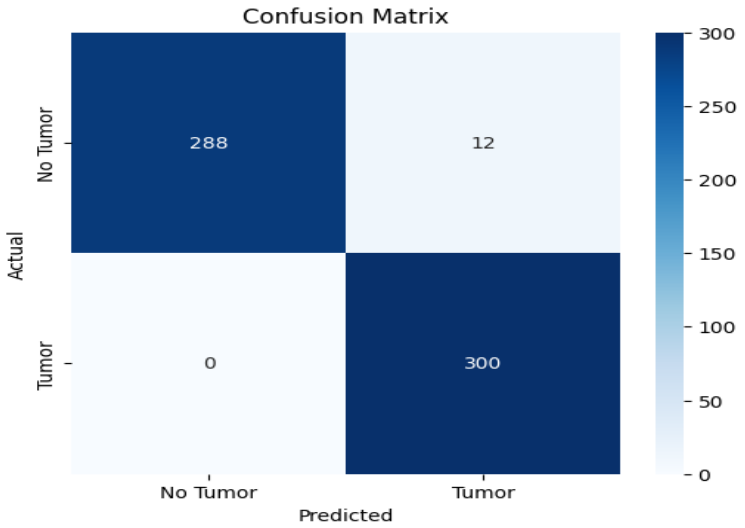

Figure 4: CNN (Learning from Scratch) confusion matrix

The training accuracy increases effortlessly and stabilizes around 95%. Validation accuracy is also high, with a 90% score and not deviating too far, which means your model generalizes well. The gap between training and validation is sensible, but no huge overfitting has been mitigated. Figure 5 shows the training and validation accuracy curve.

The training loss declines steadily and stabilizes around 0.2–0.25. Validation loss is a bit noisier but generally going downward and staying well below 0.5. The gap between the training and validation losses was slightly associated with regularization before it improved. Figure 6 below shows the training and validation loss curve.

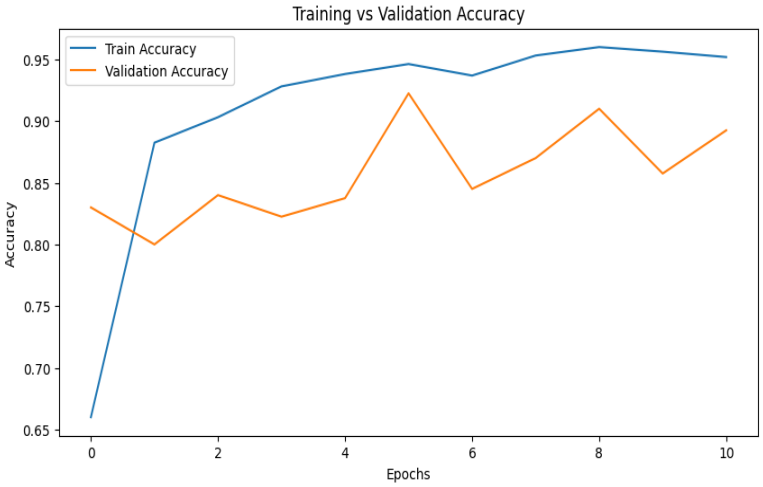

Figure 5: CNN (Training VS Validation) Accuracy Curve

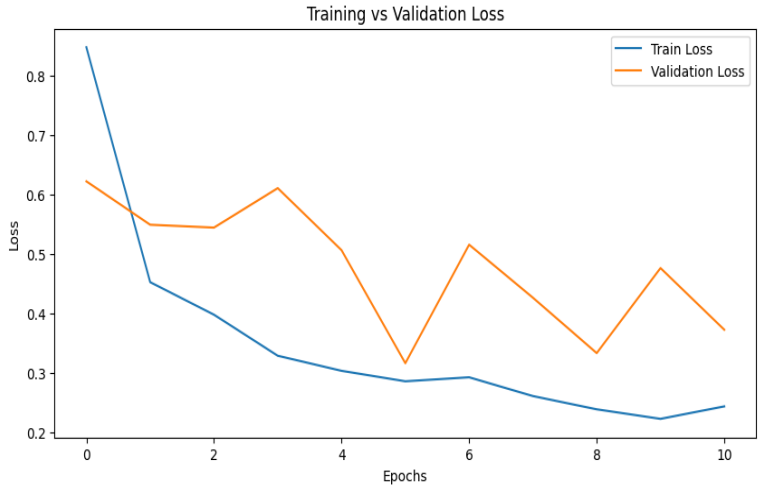

Figure 6: CNN (Training VS Validation) Loss Curve

6.3.DenseNet121 Transfer Learning

The DenseNet121 [94] with transfer learning also attained 98% accuracy with 99% sensitivity and 97% precision. Stability among sensitivity-precision shows that DenseNet121 generalized efficiently, with low positives (false) and negatives (false). 97% specificity supports the reliability of this DL model in categorizing non-tumor images. DenseNet's feature reusability and condensed connectivity pattern resulted in superior generalization compared to the baseline CNN. This is shown in Figure 7.

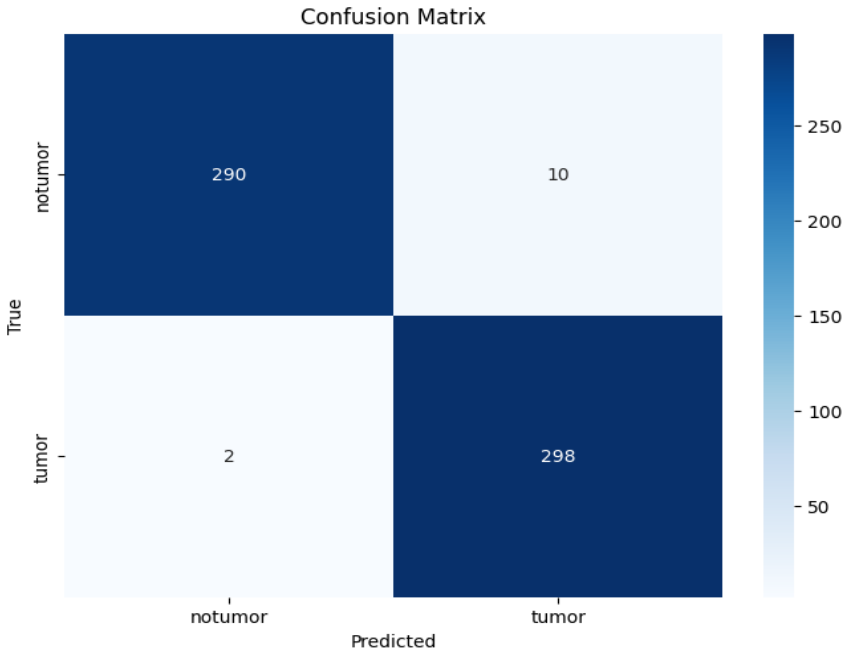

Figure 7: DenseNet121 (Transfer Learning) Confusion Matrix

Training accuracy developed gradually, reaching 93–94% by epoch 14. Validation accuracy increases rapidly, stabilizes at 98–99%, and remains outstanding after epoch 2. The model generalizes well, as validation accuracy consistently exceeds training accuracy. No overfitting because validation accuracy does not decline as epochs progress. Figure 8(a) shows the model's learning accuracy graph.

Training loss declines gradually from 1.05 to below 0.15 in 14 epochs. Validation loss decreased abruptly early on and stabilized at around 0.05, lower than the training loss. The gap between the training and validation losses indicates strong generalization without excessive overfitting. Even declining movement in both curves shows stable convergence of the DenseNet121 model. Figure 8(b) shows the model's loss graph.

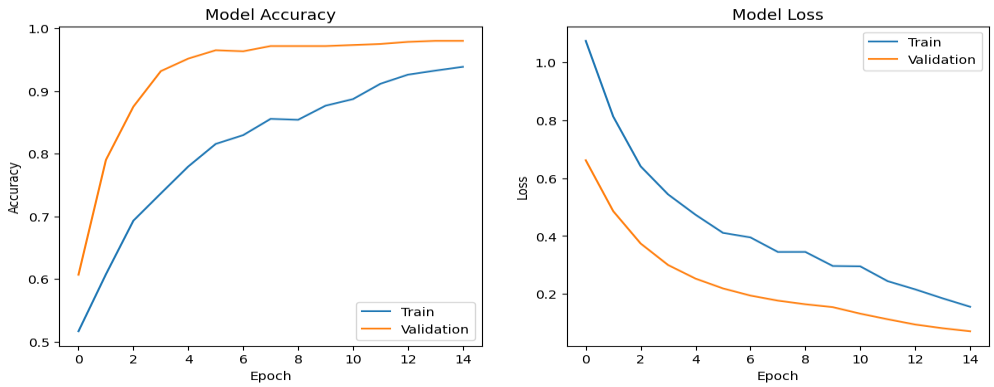

Figure 8(a) DenseNet121 Model Accuracy Graph *Figure 8 (b) DenseNet121 Model Loss Graph*

6.4.InceptionV3 Transfer Learning

InceptionV3 got 98% in all metrics (accuracy, sensitivity, precision, F1-score, and specificity). These results confirm that the model does not favor one class over the other. This made the model well-suited for medical applications in which both sensitivity and specificity are of similar importance. Critical role may have played in taking heterogeneous shapes and sizes through the multi-scale feature-extraction ability of InceptionV3, which led to steady metric results. The results are shown in Figure 9.

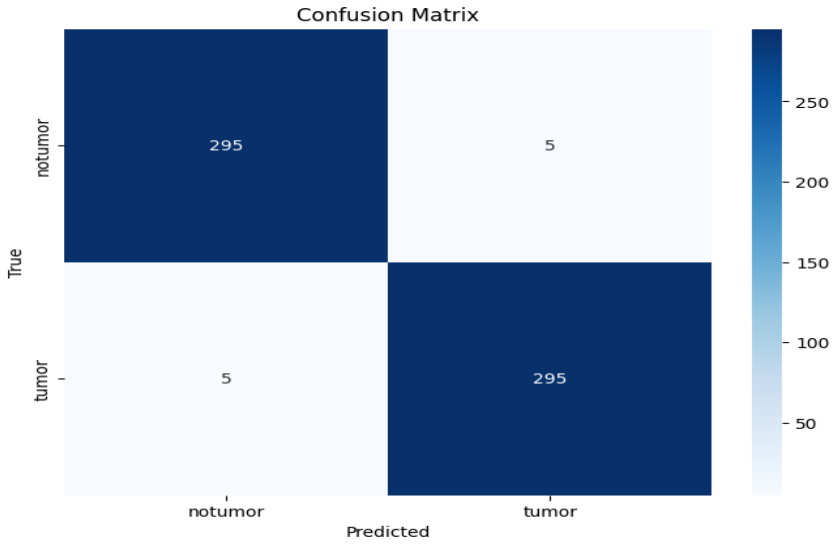

Figure 9: InceptionV3 (Transfer Learning) Confusion Matrix

The model shows a high increase in training accuracy in the early epochs, reaching 95% in epoch 6, and then stabilizes. Test accuracy remains consistently high compared to training, at about 98%, indicating solid generalization. Both curves approach stability with small fluctuations, indicating that the model is well-trained without overfitting. Accuracy is above 97–98%, which shows the efficiency of transfer learning with InceptionV3. Figure 10(a) shows the training and testing accuracy of the model.
Training loss declined abruptly at the start and has continued to decrease gradually, indicating efficient learning. Test loss shows a descending trend and stabilizes around 0.05, which is remarkably low. Test loss is gradually lower than training loss, suggesting that the InceptionV3 model generalizes well. Both curves flatten after epoch 8, showing that the model has converged successfully. Figure 10(b) shows the training and testing loss of the model.

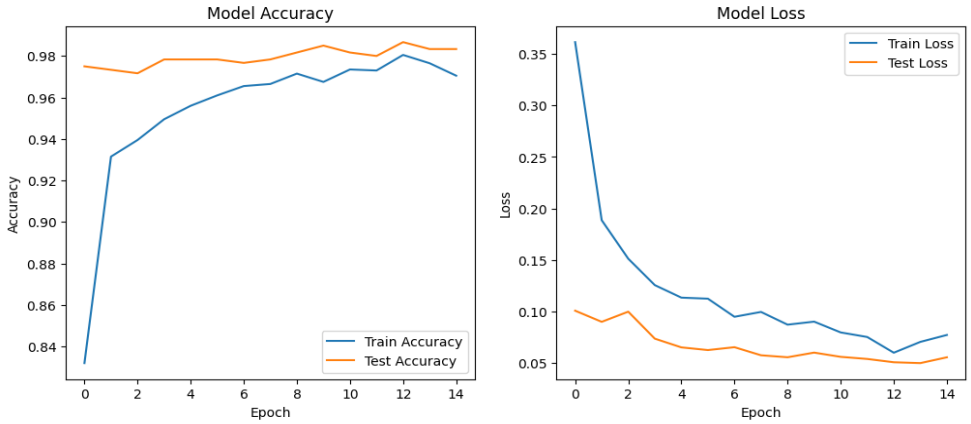

Figure 10(a) InceptionV3 Model Accuracy Graph *Figure 10(b) InceptoinV3 Model Loss Graph*

6.5.ResNet50 Transfer Learning

The Deep Learning model ResNet50 performed worse than the other models, achieving 98% accuracy, but the other metrics were low: sensitivity (86%), precision (80%), F1-score (83%), and specificity (79%). These results suggest that ResNet50 generalizes poorly on the given dataset, leading to missed tumor images (false negatives) and misclassifying healthy images (false positives). Although ResNet50 is considered an impressive model due to its outstanding architecture, in its current state it may be prone to overfitting or inadequacy. These metrics' results underscore the importance of choosing models that align perfectly with the data characteristics, rather than relying solely on model depth or approval. Figure 11 shows the confusion matrix for ResNet-

50.

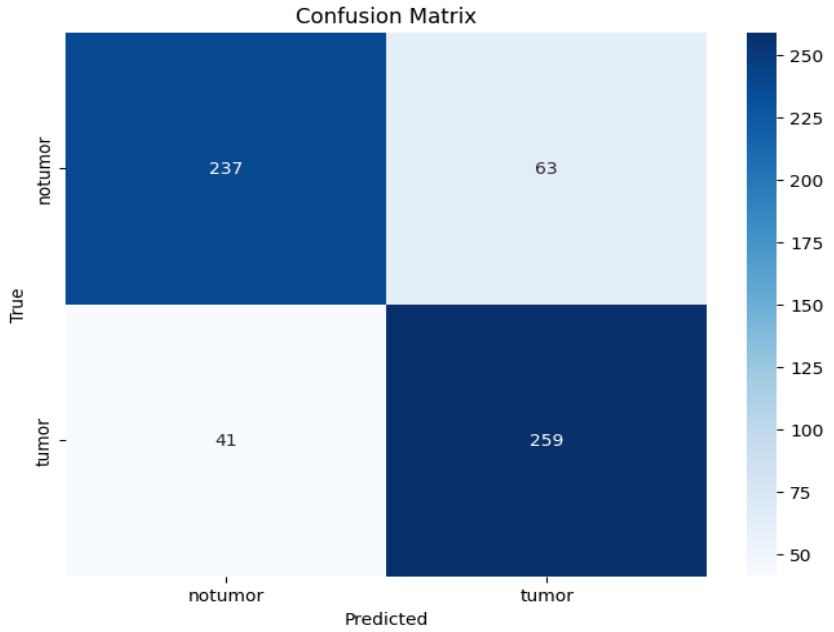

Figure 11: ResNet50 (Transfer Learning) Confusion Matrix

Training accuracy increased rapidly at the start and then stabilized above 85%, which suggests that the model is learning satisfactorily from the dataset. Validation accuracy was between 70–77%, consistently lower than training accuracy. The gap between training and validation accuracy indicates the likelihood of overfitting. Validation accuracy fluctuates after 10 epochs, then becomes comparatively stable. Figure 12(a) shows the training and testing accuracy of the model.

Training loss drops easily from 0.70 to 0.32, showing effective optimization. Validation loss shows fluctuations and remains higher than training loss, presenting some generalization glitches. The deviation between the training and validation loss curves indicates overfitting. In later epochs, the validation loss decreases slightly, suggesting the possibility of growth with regularization. Figure 12(b) shows the model's training and testing losses.

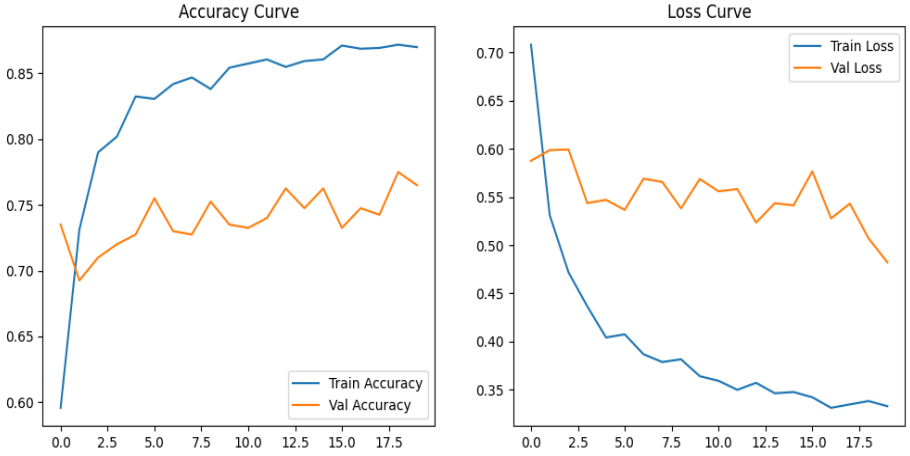

Figure 12(a): ResNet50 Model Accuracy Graph *Figure 12(b) ResNet50 Model Loss Graph*

6.6.VGG16 Transfer Learning

VGG16 proved to be the optimal performer among all models, achieving a perfect score of 100% across all metrics. This showed that all tumor and healthy MRI scans were categorized correctly with no mistakes. Instead of being an old model, VGG16 is known for extracting highly discriminative features. This pinpointed the model's suitability for

a medical image categorization task where texture (i.e., surface) and physical patterns (e.g., shapes) are very important. Despite these perfect results, they may raise concerns about possible overfitting; they found VGG16 to be the most reliable model in this experimental setup. Figure 13 below shows the outcomes.

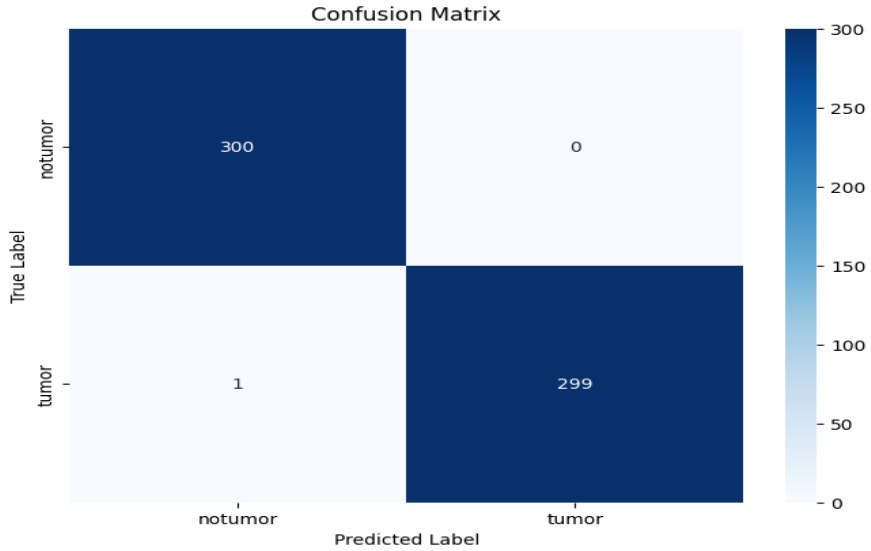

Figure 13: VGG16 (Transfer Learning) Confusion Matrix

Training accuracy increased rapidly from 91% to 97%, showing that the VGG-16 Deep Learning model learned effective structures early. Validation accuracy is progressively higher, reaching 98%–100%, indicating generalization. Both curves plateau after epoch 7, showing the model has converged. Training and validation curves are very close, with validation slightly better than training. Figure 14(a) shows the training and testing accuracy of the model.

Training loss drops suddenly at the start, indicating fast learning. Validation loss remains small and below training loss, showing perfect generalization. Both training and validation losses are steady at very low values, 0.01–0.02. Deviation was nil between the training and validation losses, indicating that the model is not overfitting despite the high accuracy. Figure 14(b) shows the model's training and testing losses.

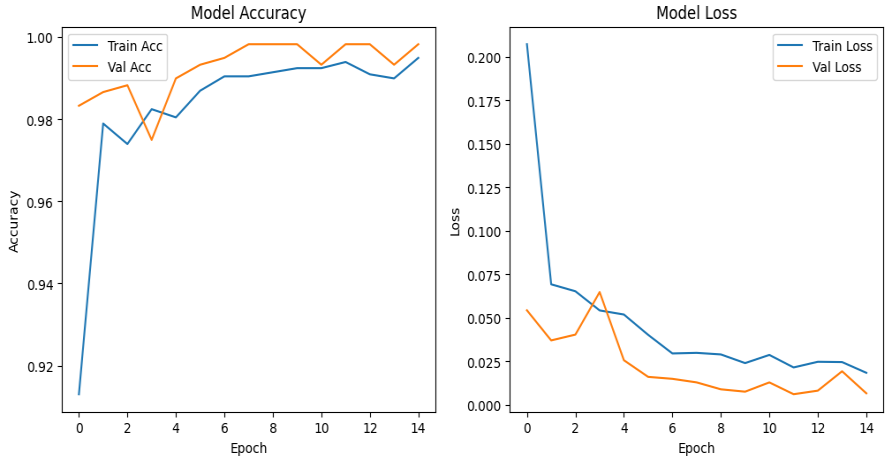

Figure 14(a): VGG16 Model Accuracy Graph

Figure 14(b): VGG16 Model Loss Graph

7. Overall Discussion

Results show that, although all DL models performed well, each model's strong points differ across metrics. CNN (learning from scratch) demonstrated efficiency, confirming the competence of training on the specific dataset without the use of external pre-trained weights. On the other hand, DenseNet121 and InceptionV3 exhibit stable generalization, which reflects the advantage of transfer learning due to their rich feature

representations. Moreover, ResNet50, despite its depth and architectural novelties, yielded less-effective results. VGG16 outperformed the other DL models, achieving perfect classification results across all assessment metrics.
The results showed that, in medical image classification, the choice of DL models is not only dependent on experimental validation across multiple performance indicators but also on architectural complexity. DL models, e.g., VGG16 and InceptionV3, stand out for their steady, reliable classification performance in clinical applications, whereas ResNet50 may require additional fine-tuning or data augmentation to strengthen its performance.

7.1.LIME Explanation on VGG16 (Best Model)

The following figure provides a spatial visualization of the LIME explanation for a tumor on an MRI scan, complementing the quantitative features shown in Figure 15. The three pictures demonstrate the model's decision, with increasing levels of detail, by highlighting the top 5, 10, and 15 most effective super pixels. The emphasized regions, mainly the essential areas present in all three pictures, specify the image features that the VGG16 model relies on for classification. Significantly, these regions are particularly intense in the abnormal brain tissue, indicating that the model's decision-making is clinically reasonable and associated with radiological awareness. This visual contract between the AI's explanation and the predictable pathological location is vital for confirming the model's trustworthiness and building trust for probable clinical use.

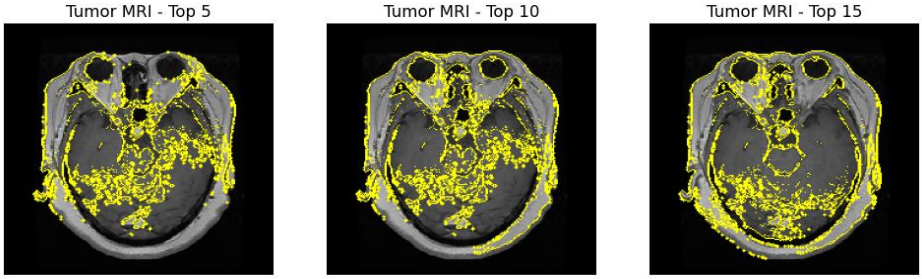

Figure 15(a): LIME Explainability on Top 5 Figure15(b): LIME Explainability on Top 10 Figure 15(c) LIME Explainability on Top 15

The LIME scrutiny, as shown in Figure 16, provides a post-hoc explanation of the AI model's decision for a specific Tumor MRI. This procedure identifies which sections of the scan were most persuasive in the decision-making process by segmenting the MRI into clear super pixels and then assessing their individual influence. The bar chart clearly positions these features by their rank. For this specific prediction, Super pixel 18 was the most important positive contributor, strongly driving the model toward the tumor result. This was then followed by other crucial sections, such as Super pixels 14, 33, and 29. This picturing is critical for building confidence and transparency because it allows clinicians to verify that the model is focusing on clinically pertinent areas rather than on inappropriate or false noise in the image.

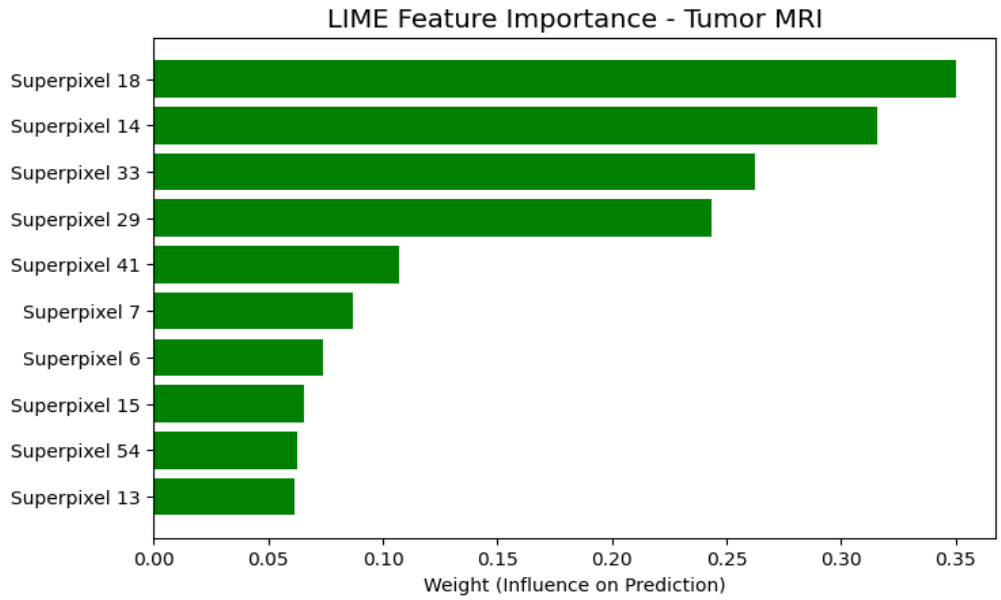

Figure 16: LIME Feature Importance - Tumor MRI

Figure 17 below shows the LIME explanation for an appropriately classified non-tumor MRI scan, which illustrates the image areas that most significantly contributed to the model's negative decision. The super pixels highlighted as the top 5, 10, and 15 most effective features are not concentrated in a central abnormal area but are distributed across various regions of the normal brain. This pattern specifies that the model's decision was based entirely on the positive identification of healthy anatomical features, rather than on the mere absence of a tumor. The uniformity of these highlights across all panels validates that the model has established a robust internal depiction of a healthy brain on MRI. This capability to recognize normality is a critical feature of the model's trustworthiness, as it helps reduce false-positive diagnoses.

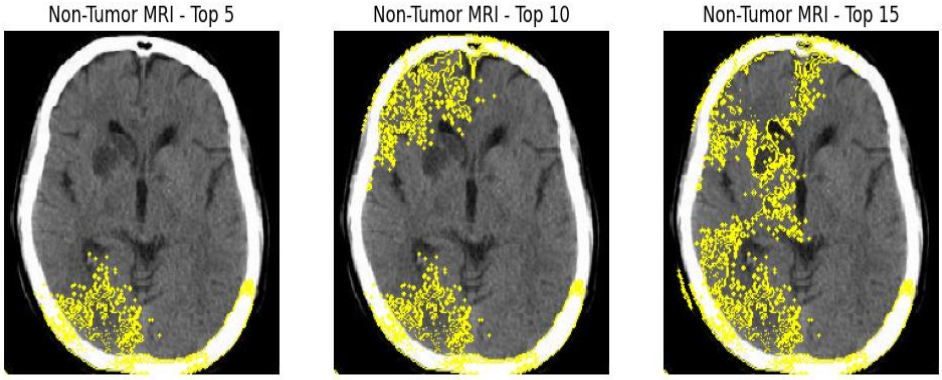

Figure 17(a): LIME Explainability on Top 5 Figure17(b): LIME Explainability on Top 10 Figure 17(c) LIME Explainability on Top 15

Figure 18 illustrates the LIME explanation for the model's prediction for an MRI scan appropriately categorized as healthy (non-tumor). This examination discloses the scan image areas that most strongly suggest the model discarded a tumor verdict. Unlike the positive weights observed in the tumor case, the super pixels here show negative weights because they indicate that their occurrence reduces the model's certainty of a positive tumor result. The super pixel 89 was the most prominent feature, serving as the strongest indicator of healthy tissue in the MRI scan. This result was also supported by other areas, e.g., Super pixels 74 and 20. All of these together provided a graphic indication of non-tumor tissue. The ability to recognize features related to healthy MRI is equally important because it not only validates that the model is not merely diagnosing tumors but also detecting the presence of normal brain tissue, thereby

reducing the probability of false-positive detections.

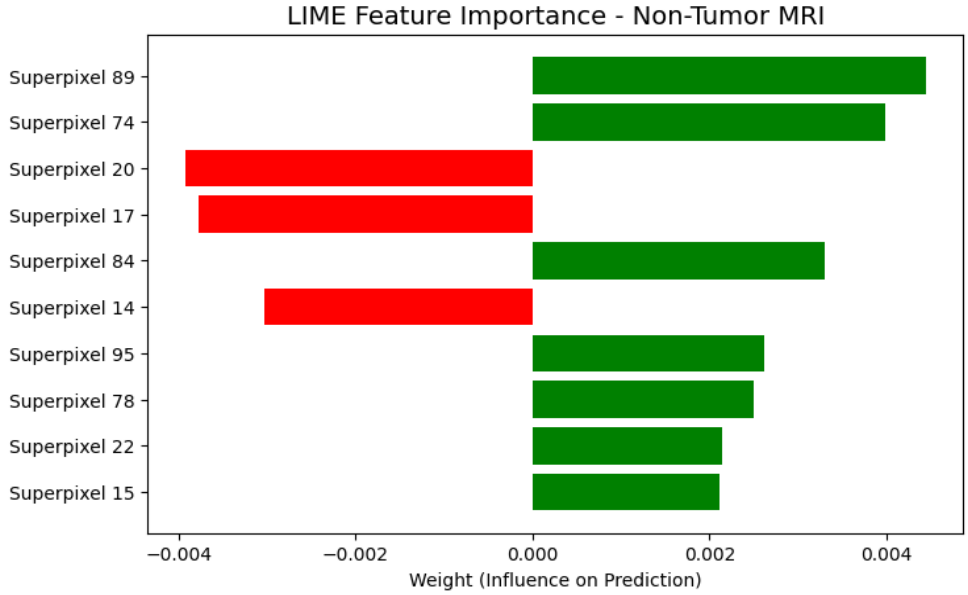

Figure 18: LIME Feature Importance - Non-Tumor MRI

7.2.SHAP (SHapley Additive exPlanations) Explanation on VGG16 (Best Model)

The heatmap in Figure 19 (Tumor MRI - SHAP Heatmap) explains why the VGG16 model classified the MRI scan as a Tumor. The areas shaded in red (with positive SHAP values around 0.075) highlight the pixels that were the most important positive contributors to the Tumor prediction result. These areas have pictorial patterns that these models have learned are highly revealing of tumorous tissue, such as irregular shapes and textures.

The regions shaded in blue (with negative SHAP values around -0.075) indicate pixels that would have been classified against a tumor prediction result. In the context of a tumor image, these likely denote regions of normal, healthy brain, such as white or grey matter. The model appropriately classifies their occurrence as unpredictable in the presence of a prevalent tumor, but their effect is outweighed by the robust positive evidence from those red areas.

This permits clinicians to authenticate that the model's results are clinically reasonable. If the red hotspots align with radiologically confirmed tumor areas, this builds trust in the decision-making process. It determines that the model is not relying on inappropriate image artifacts or biases but is focusing on pathologically pertinent regions.

Figure 20 (Non-Tumor MRI - SHAP Heatmap) shows why the model correctly classified a different MRI-scanned image as non-tumor. The main regions here are those with the strong negative SHAP values (e.g., the blue sections, with a prominent value of -0.100). These pixels are the most significant indication of the nonappearance of a tumor. They denote features of healthy composition. Their presence powerfully reduced the model's score for the tumor class.

To understand the prediction results of our best model (VGG16) and to ensure its clinical credibility, we applied SHAP analysis. SHAP measures the contribution of each feature (e.g., a pixel) to the final result, providing a detailed explanation (e.g., pixel-level). As can be seen in Figure 19 (Tumor MRI - SHAP Heatmap), for an MRI scan correctly classified as a tumor, the SHAP heatmap highlights specific areas in red with high positive values, indicating that they were the principal drivers of the tumor detection. These regions align well with radiologically doubtful areas, thereby confirming the model's emphasis on clinically applicable features. On the contrary, Figure 20 (Non-Tumor MRI - SHAP Heatmap) illustrates a non-tumor prediction result, where specific regions with strong, high negative SHAP values, represented in blue,

indicate features of healthy/normal structure that actively reduced the tumor classification score, representing the model's learned depiction of normality. These high levels of interpretability are important not only for building trust but also for enabling clinical implementation by allowing experts to validate the model's decision-making process against their own field knowledge. Figure 21 shows the class contributions for the tumor image, while Figure 22 shows the class contributions for the tumor image.

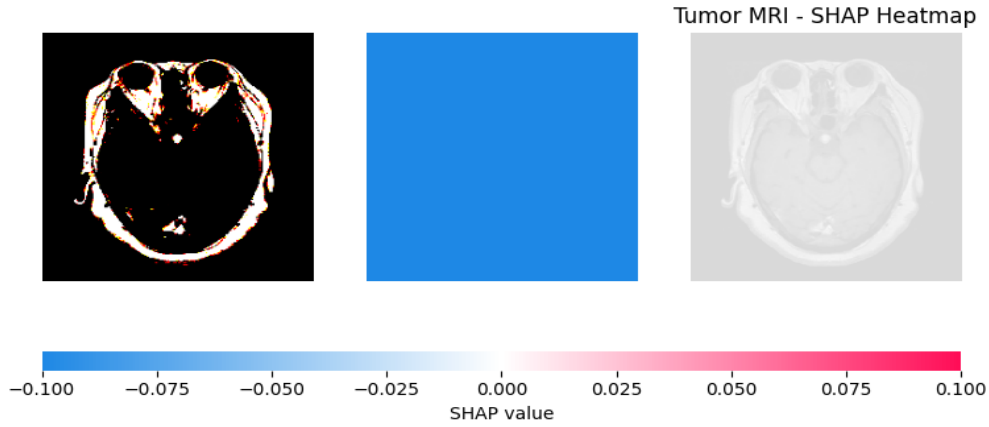

Figure 19: SHAP Explainability Heatmap, Tumor MRI

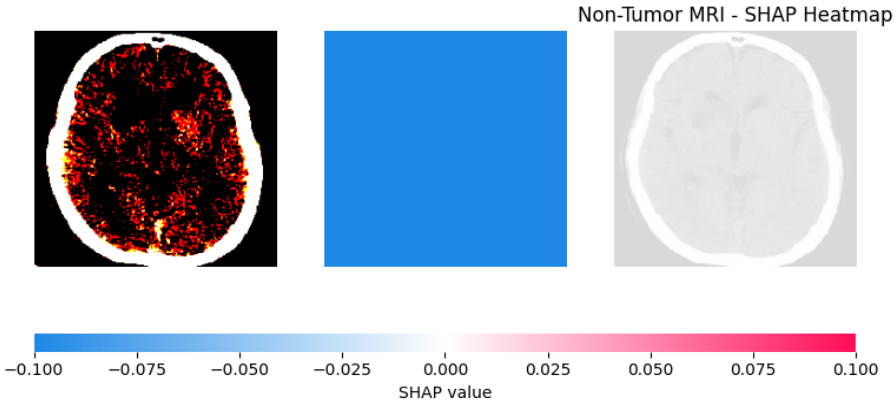

Figure 20: Figure 19: SHAP Explainability Heatmap, Non-Tumor MRI

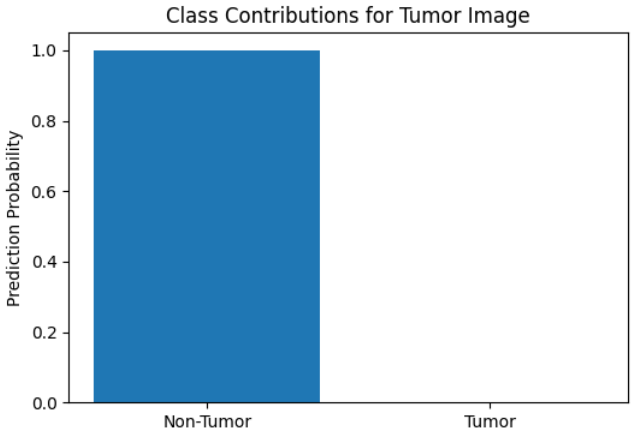

Figure 21: Class Contributions for Tumor Image

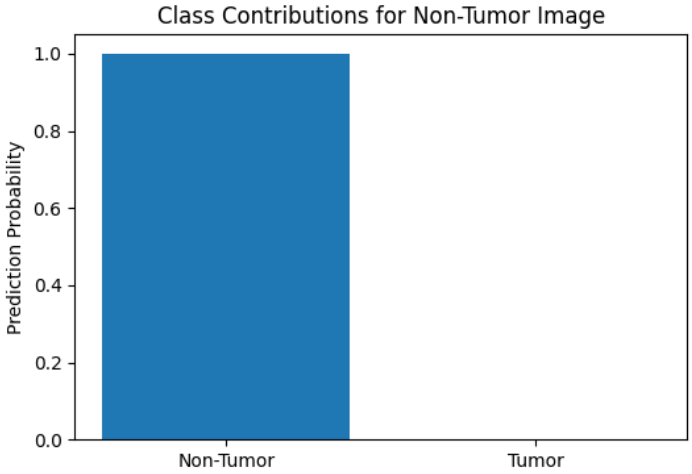

Figure 22: Class Contributions for Non-Tumor Image

8. Results and Discussion

This specific unit presents the results of DL models applied to brain tumor categorization and discusses their implications. We assessed five DL models (CNN trained from scratch, DenseNet121, InceptionV3, ResNet50, and VGG16) on a dataset containing 2,000 training brain scans (1,000 tumor and 1,000 healthy) and 600 testing brain scans (300 tumor and 300 healthy) on the metrics, e.g., accuracy, sensitivity, precision, F1 score, and specificity.

8.1.Results Comparison of DL Models

Quantitative results revealed that all DL models tested in the study achieved high overall accuracy, with VGG16 achieving the best score of 100% across all metrics. CNN from scratch, as well as InceptionV3, got 98% of accuracy. Here, the CNN showed 100% sensitivity but lower precision at 96%. This showed that a slight rate of false-positive guesses was observed. The DenseNet121 achieved a steady accuracy of 98%, sensitivity of 99%, and precision of 97%, indicating that its efficacy extends beyond feature extraction to gradient propagation. ResNet50, even though preserving high overall accuracy (98%), exhibited lower sensitivity (86%) and precision (80%), resulting in less consistent identification of tumor scans.

The pictorial visualizations of results, e.g., the bar and radar charts, provide an amusing visual representation of model outcomes. VGG16 consistently outperformed across all metrics, while ResNet50 showed clear gaps in sensitivity and precision. DenseNet121 and InceptionV3 produce reliable, consistent results, but still underachieve compared with VGG16. These results suggested that classification performance is enhanced when using transfer learning, specifically with VGG16, compared to learning from scratch.

8.2. Analysis of Model Characteristics

VGG16 enables well-organized feature extraction while preserving model simplicity, and its higher performance can be attributed to its uniform 3×3 convolutional architecture. The DenseNet121 model uses dense connectivity, which improves gradient flow and feature reuse. InceptionV3 has multi-scale convolutional layers with characteristics at different resolutions, which, in turn, strengthen dynamic brain tumor detection. ResNet50's enduring connections appear less suitable for the current dataset, although designed to improve training in very deep networks, as it showed lower sensitivity and precision.

8.3.Implications for Brain Cancer Classification

These results showed that CNN (trained from scratch) was beaten by DL transfer learning models, with the VGG16 model being the most consistent for accurate brain

cancer categorization. Misclassification of brain tumors in medical diagnosis is greatly dependent on sensitivity and precision. The stable and best results of VGG16 across all assessment metrics suggest that this model is suitable for integration with explainable AI-based approaches (e.g., LIME and SHAP) to deliver explainable calculations, which will, in turn, improve clinical applicability and trustworthiness.

8.4. Overall Observations

Generally, it is observed that DL models (learning from scratch and transfer learning) actually effect the classification of brain scans through the proportional assessment. Transfer learning quickens this process and improves accuracy and steadiness, especially in situations where datasets are limited, e.g., in size, as is the case with the current MRI dataset. VGG16's best performance across all selected metrics makes it the ideal model for the explainable AI examination, as well as for possible placement in clinical decision support systems in real-life environments.

8.5.Conclusion and Future Work

This research work examined the performance of DL models for brain cancer classification using a dataset of MRI brain scans. The models include those trained from scratch (CNN) and transfer learning (DenseNet121, InceptionV3, ResNet50, and VGG16). This quantitative work confirmed that all these DL models achieved high accuracy, while VGG16 consistently outperformed all other DL models, attaining perfect scores of 100% across Accuracy, Sensitivity, Precision, F1 Score, and Specificity. The quantitative results highlighted the efficacy of transfer learning due to the availability of pre-trained feature representations. This strategy not only improves categorization performance but also reduces computational cost and training time compared with the learning-from-scratch method.

These results highlighted the strengths of each model. DenseNet121 performed well because of its dense connections, which encourage feature reuse. While the InceptionV3 successfully took multi-scale characteristics. On the other hand, ResNet50 presented inferior sensitivity and precision on this brain MRI scans dataset despite its deep residual architecture. After applying explainable AI-based techniques, e.g., LIME and SHAP, we obtained interpretable insights into VGG16's predictions, thereby ensuring transparency, consistency, and building trust, which are crucial for a medical diagnostic system in clinics.

Future work will mainly focus on enhancing the dataset (MRI scans) by including a wider range of MRI images from multiple institutions to improve the model's generalization and robustness. Moreover, integrating multi-source imaging datasets, e.g., CT scans and PET images, with MRI could further improve the accuracy and consistency of brain cancer classification. Further research will also identify hybrid models that combine DL with classical ML methods and progressive explainable AI agendas to provide clinicians with more actionable insights, eventually helping to generate initial findings and modified treatment approaches for brain tumor patients.

Ethics Approval

This study used publicly available datasets that were fully anonymized before access. No human participants were directly involved, and no identifiable information was used. Therefore, ethical approval was not required for this research.

Consent to participate

Not applicable, as the study involved only secondary analysis of anonymized, publicly available data.

Acknowledgement

The authors would like to thank the original dataset providers for making the data publicly available, which enabled this research.

Competing Interests

The authors declare there are no competing interests

Author Contributions

- Asif Rahman was responsible for dataset selection and model training, ensuring the experimental framework aligned with the research objectives.
- Maqsood Hayat conceived and designed the experiments, performed the experiments, analyzed the data, performed the computation work, prepared figures and/or tables, authored and reviewed drafts of the article, and approved the final draft.
- Hashim Ali conducted the dataset preprocessing, including data cleaning and transformation, performed the experiments, analyzed the data, and performed the computation work.

Clinical Trial Number

Not applicable

Funding

This research received no external funding.

Dataset and Code availability

The dataset analyzed in this research study is publicly available at the Brain Tumor MRI Dataset and code is available at GitHub - asifrahman557/Explainable-AI-using-SHAP-LIME · GitHub

REFERENCES

1. Qureshi, S.A., et al., *Intelligent ultra-light deep learning model for multi-class brain tumor detection.* Applied Sciences, 2022. 12(8): p. 3715.
2. Mumtaz Zahoor, M., et al., *A New Deep Hybrid Boosted and Ensemble Learning-based Brain Tumor Analysis using MRI.* arXiv e-prints, 2022: p. arXiv: 2201.05373.
3. Arabahmadi, M., R. Farahbakhsh, and J. Rezazadeh, *Deep learning for smart Healthcare—A survey on brain tumor detection from medical imaging.* Sensors, 2022. 22(5): p. 1960.
4. Prabukumar, M., L. Agilandeeswari, and K. Ganesan, *An intelligent lung cancer diagnosis system using cuckoo search optimization and support vector machine classifier.* Journal of ambient intelligence and humanized computing, 2019. 10(1): p. 267-293.
5. Tandel, G.S., et al., *A review on a deep learning perspective in brain cancer classification.* Cancers, 2019. 11(1): p. 111.
6. Raut, G., et al. *Deep learning approach for brain tumor detection and segmentation*. in *2020 International Conference on Convergence to Digital World-Quo Vadis (ICCDW)*. 2020. IEEE.
7. DeAngelis, L.M., *Brain tumors.* New England journal of medicine, 2001. 344(2): p. 114-123.
8. Borole, V.Y., S.S. Nimbhore, and D.S.S. Kawthekar, *Image processing techniques for brain tumor detection: A review.* International Journal of Emerging Trends & Technology in Computer Science (IJETTCS), 2015. 4(5): p. 2.
9. Amin, J., et al., *Big data analysis for brain tumor detection: Deep convolutional neural networks.* Future Generation Computer Systems, 2018. 87: p. 290-297.
10. Iorgulescu, J.B., et al., *Molecular biomarker-defined brain tumors: epidemiology, validity, and completeness in the United States.* Neuro-oncology, 2022. 24(11): p. 1989-2000.
11. Mabray, M.C., R.F. Barajas Jr, and S. Cha, *Modern brain tumor imaging.* Brain tumor research and treatment, 2015. 3(1): p. 8.
12. Cha, S., *Update on brain tumor imaging: from anatomy to physiology.* American Journal of Neuroradiology, 2006. 27(3): p. 475-487.

13. Ranjbarzadeh, R., et al., *Brain tumor segmentation based on deep learning and an attention mechanism using MRI multi-modalities brain images.* Scientific reports, 2021. 11(1): p. 10930.
14. Saba, T., et al., *Brain tumor detection using fusion of hand crafted and deep learning features.* Cognitive Systems Research, 2020. 59: p. 221-230.
15. El-Dahshan, E.-S.A., et al., *Computer-aided diagnosis of human brain tumor through MRI: A survey and a new algorithm.* Expert systems with Applications, 2014. 41(11): p. 5526-5545.
16. Meng, Y., et al., *Exposure to lead increases the risk of meningioma and brain cancer: A meta-analysis.* Journal of Trace Elements in Medicine and Biology, 2020. 60: p. 126474.
17. McFaline-Figueroa, J.R. and E.Q. Lee, *Brain tumors.* The American journal of medicine, 2018. 131(8): p. 874-882.
18. Chavan, N.V., B. Jadhav, and P. Patil, *Detection and classification of brain tumors.* International Journal of Computer Applications, 2015. 112(8): p. 48-53.
19. Amin, J., et al., *Brain tumor detection and classification using machine learning: a comprehensive survey.* Complex & intelligent systems, 2022. 8(4): p. 3161-3183.
20. Chhabda, S., et al., *The 2016 World Health Organization classification of tumours of the central nervous system: what the paediatric neuroradiologist needs to know.* Quantitative imaging in medicine and surgery, 2016. 6(5): p. 486.
21. Badža, M.M. and M.Č. Barjaktarović, *Classification of brain tumors from MRI images using a convolutional neural network.* Applied Sciences, 2020. 10(6): p. 1999.
22. Rahman, A., et al., *Enhanced MRI brain tumor detection using deep learning in conjunction with explainable AI SHAP based diverse and multi feature analysis.* Scientific Reports, 2025. 15(1): p. 29411.
23. Tiwari, P., et al., *Cnn based multiclass brain tumor detection using medical imaging.* Computational Intelligence and Neuroscience, 2022. 2022(1): p. 1830010.
24. Anaya-Isaza, A. and L. Mera-Jiménez, *Data augmentation and transfer learning for brain tumor detection in magnetic resonance imaging.* IEEE access, 2022. 10: p. 23217-23233.
25. Lotlikar, V.S., N. Satpute, and A. Gupta, *Brain tumor detection using machine learning and deep learning: a review.* Current Medical Imaging Reviews, 2022. 18(6): p. 604-622.
26. Xie, Y., et al., *Convolutional neural network techniques for brain tumor classification (from 2015 to 2022): Review, challenges, and future perspectives.* Diagnostics, 2022. 12(8): p. 1850.
27. Guyon, I. and A. Elisseeff, *An introduction to variable and feature selection.* Journal of machine learning research, 2003. 3(Mar): p. 1157-1182.
28. Rana, M. and M. Bhushan, *Machine learning and deep learning approach for medical image analysis: diagnosis to detection.* Multimedia Tools and Applications, 2023. 82(17): p. 26731-26769.
29. Almadhoun, H.R. and S.S. Abu-Naser, *Detection of brain tumor using deep learning.* 2022.
30. Musallam, A.S., A.S. Sherif, and M.K. Hussein, *A new convolutional neural network architecture for automatic detection of brain tumors in magnetic resonance imaging images.* IEEE access, 2022. 10: p. 2775-2782.
31. Nayak, D.R., et al., *Brain tumor classification using dense efficient-net.* Axioms, 2022. 11(1): p. 34.
32. Obeidavi, M.R. and K. Maghooli. *Tumor detection in brain MRI using residual convolutional neural networks*. in *2022 International conference on machine vision and image processing (MVIP)*. 2022. IEEE.

33. Khalil, H.A., et al., *3D-MRI brain tumor detection model using modified version of level set segmentation based on dragonfly algorithm.* Symmetry, 2020. 12(8): p. 1256.
34. Sajid, S., S. Hussain, and A. Sarwar, *Brain tumor detection and segmentation in MR images using deep learning.* Arabian Journal for Science and Engineering, 2019. 44(11): p. 9249-9261.
35. Zhuang, Y., et al., *An Effective WSSENet-Based Similarity Retrieval Method of Large Lung CT Image Databases.* KSII Transactions on Internet & Information Systems, 2022. 16(7).
36. Liu, Z., et al., *Instant diagnosis of gastroscopic biopsy via deep-learned single-shot femtosecond stimulated Raman histology.* Nature communications, 2022. 13(1): p. 4050.
37. Litjens, G., et al., *A survey on deep learning in medical image analysis.* Medical image analysis, 2017. 42: p. 60-88.
38. Chaturvedi, P., et al. *Prediction and classification of lung cancer using machine learning techniques*. in *IOP conference series: materials science and engineering*. 2021. IOP Publishing.
39. Liu, H., et al., *Recent advances in pulse-coupled neural networks with applications in image processing.* Electronics, 2022. 11(20): p. 3264.
40. Zhuang, Y., N. Jiang, and Y. Xu, *Progressive distributed and parallel similarity retrieval of large CT image sequences in mobile telemedicine networks.* Wireless communications and mobile computing, 2022. 2022(1): p. 6458350.
41. Pashaei, A., H. Sajedi, and N. Jazayeri. *Brain tumor classification via convolutional neural network and extreme learning machines*. in *2018 8th International conference on computer and knowledge engineering (ICCKE)*. 2018. IEEE.
42. Rehman, A., et al., *A deep learning-based framework for automatic brain tumors classification using transfer learning.* Circuits, Systems, and Signal Processing, 2020. 39(2): p. 757-775.
43. Paul, J.S., et al. *Deep learning for brain tumor classification*. in *Medical Imaging 2017: Biomedical Applications in Molecular, Structural, and Functional Imaging*. 2017. SPIE.
44. Noreen, N., et al., *A deep learning model based on concatenation approach for the diagnosis of brain tumor.* IEEE access, 2020. 8: p. 55135-55144.
45. Asiri, A.A., et al., *Machine learning-based models for magnetic resonance imaging (MRI)-based brain tumor classification.* Intell. Autom. Soft Comput, 2023. 36: p. 299-312.
46. Abbas, K., et al. *Automatic brain tumor detection in medical imaging using machine learning*. in *2019 International conference on information and communication technology convergence (ICTC)*. 2019. IEEE.
47. Siar, M. and M. Teshnehlab. *Brain tumor detection using deep neural network and machine learning algorithm*. in *2019 9th international conference on computer and knowledge engineering (ICCKE)*. 2019. IEEE.
48. Rehman, Z.U., et al., *Texture based localization of a brain tumor from MR-images by using a machine learning approach.* Medical hypotheses, 2020. 141: p. 109705.
49. Al-Haija, Q.A., M. Smadi, and O.M. Al-Bataineh. *Early stage diabetes risk prediction via machine learning*. in *International Conference on Soft Computing and Pattern Recognition*. 2021. Springer.
50. Arunprasath, T., M.P. Rajasekaran, and G. Vishnuvarathanan. *MR Brain image segmentation for the volumetric measurement of tissues to differentiate Alzheimer's disease using hybrid algorithm*. in *2019 IEEE International Conference on Clean Energy and Energy Efficient Electronics Circuit for Sustainable Development (INCCES)*. 2019. IEEE.

51. Dixit, A. and A. Nanda. *Brain MR image classification via PSO based segmentation*. in *2019 Twelfth International Conference on contemporary computing (IC3)*. 2019. IEEE.
52. Korolev, S., et al. *Residual and plain convolutional neural networks for 3D brain MRI classification*. in *2017 IEEE 14th international symposium on biomedical imaging (ISBI 2017)*. 2017. IEEE.
53. Sangeetha, R., et al. *Automatic detection of brain tumor using deep learning algorithms*. in *2020 4th International Conference on Electronics, Communication and Aerospace Technology (ICECA)*. 2020. IEEE.
54. Latif, G., et al., *Glioma Tumors' classification using deep-neural-network-based features with SVM classifier.* Diagnostics, 2022. 12(4): p. 1018.
55. Anaraki, A.K., M. Ayati, and F. Kazemi, *Magnetic resonance imaging-based brain tumor grades classification and grading via convolutional neural networks and genetic algorithms.* biocybernetics and biomedical engineering, 2019. 39(1): p. 63-74.
56. Abdusalomov, A.B., M. Mukhiddinov, and T.K. Whangbo, *Brain tumor detection based on deep learning approaches and magnetic resonance imaging.* Cancers, 2023. 15(16): p. 4172.
57. Kamnitsas, K., et al., *Efficient multi-scale 3D CNN with fully connected CRF for accurate brain lesion segmentation.* Medical image analysis, 2017. 36: p. 61-78.
58. Havaei, M., et al., *Brain tumor segmentation with deep neural networks.* Medical image analysis, 2017. 35: p. 18-31.
59. Kang, J., Z. Ullah, and J. Gwak, *MRI-based brain tumor classification using ensemble of deep features and machine learning classifiers.* Sensors, 2021. 21(6): p. 2222.
60. Younis, A., et al., *Brain tumor analysis using deep learning and VGG-16 ensembling learning approaches.* Applied Sciences, 2022. 12(14): p. 7282.
61. Zahid, U., et al., *BrainNet: optimal deep learning feature fusion for brain tumor classification.* Computational Intelligence and Neuroscience, 2022. 2022(1): p. 1465173.
62. Ostrom, Q.T., et al., *CBTRUS statistical report: primary brain and other central nervous system tumors diagnosed in the United States in 2013–2017.* Neuro-oncology, 2020. 22(Supplement_1): p. iv1-iv96.
63. Han-Trong, T., et al., *An efficient method for diagnosing brain tumors based on MRI images using deep convolutional neural networks.* Applied Computational Intelligence and Soft Computing, 2022. 2022(1): p. 2092985.
64. Krizhevsky, A., I. Sutskever, and G.E. Hinton, *Imagenet classification with deep convolutional neural networks.* Advances in neural information processing systems, 2012. 25.
65. Amodei, D., et al. *Deep speech 2: End-to-end speech recognition in english and mandarin*. in *International conference on machine learning*. 2016. PMLR.
66. Collobert, R. and J. Weston. *A unified architecture for natural language processing: Deep neural networks with multitask learning*. in *Proceedings of the 25th international conference on Machine learning*. 2008.
67. Fioretto, F., et al. *Lagrangian duality for constrained deep learning*. in *Joint European conference on machine learning and knowledge discovery in databases*. 2020. Springer.
68. Vinyals, O., M. Fortunato, and N. Jaitly, *Pointer networks.* Advances in neural information processing systems, 2015. 28.
69. Khalil, E., et al., *Learning combinatorial optimization algorithms over graphs.* Advances in neural information processing systems, 2017. 30.
70. Kool, W., H. Van Hoof, and M. Welling, *Attention, learn to solve routing problems!* arXiv preprint arXiv:1803.08475, 2018.
71. Donti, P., B. Amos, and J.Z. Kolter, *Task-based end-to-end model learning in stochastic optimization.* Advances in neural information processing systems, 2017. 30.

72. Amos, B. and J.Z. Kolter. *Optnet: Differentiable optimization as a layer in neural networks*. in *International conference on machine learning*. 2017. PMLR.
73. Wilder, B., B. Dilkina, and M. Tambe. *Melding the data-decisions pipeline: Decision-focused learning for combinatorial optimization*. in *Proceedings of the AAAI conference on artificial intelligence*. 2019.
74. Hijazi, S., R. Kumar, and C. Rowen, *Using convolutional neural networks for image recognition.* Cadence Design Systems Inc.: San Jose, CA, USA, 2015. 9(1): p. 39.
75. O'shea, K. and R. Nash, *An introduction to convolutional neural networks.* arXiv preprint arXiv:1511.08458, 2015.
76. Wong, K.K., G. Fortino, and D. Abbott, *Deep learning-based cardiovascular image diagnosis: a promising challenge.* Future Generation Computer Systems, 2020. 110: p. 802-811.
77. Devanathan, B. and K. Venkatachalapathy, *Brain tumor detection and classification model using optimal Kapur's thresholding based segmentation with deep neural networks.* IIOABJ, 2020. 11(4): p. 1-8.
78. Abunasser, B.S., et al., *Breast cancer detection and classification using deep learning Xception algorithm.* International Journal of Advanced Computer Science and Applications, 2022. 13(7).
79. Abunasser, B.S., et al., *Prediction of instructor performance using machine and deep learning techniques.* International Journal of Advanced Computer Science and Applications, 2022. 13(7).
80. Abdalla, H.E.M. and M.Y. Esmail. *Brain tumor detection by using artificial neural network*. in *2018 International conference on computer, control, electrical, and electronics engineering (ICCCEEE)*. 2018. IEEE.
81. Saleh, A., R. Sukaik, and S.S. Abu-Naser. *Brain tumor classification using deep learning*. in *2020 International Conference on Assistive and Rehabilitation Technologies (iCareTech)*. 2020. IEEE.
82. Arunkumar, N., et al., *Fully automatic model-based segmentation and classification approach for MRI brain tumor using artificial neural networks.* Concurrency and Computation: Practice and Experience, 2020. 32(1): p. e4962.
83. Atieh, K., *INTEGRATION OF THE DIMENSIONS OF COMPUTERIZED HEALTH INFORMATION SYSTEMS AND THEIR ROLE IN IMPROVING ADMINISTRATIVE PERFORMANCE IN AL-SHIFA MEDICAL COMPLEX.* 2020.
84. Abu-Naser, S.S., et al., *An expert system for endocrine diagnosis and treatments using JESS.* 2010.
85. Abd-Ellah, M.K., et al., *Two-phase multi-model automatic brain tumour diagnosis system from magnetic resonance images using convolutional neural networks.* EURASIP Journal on Image and Video Processing, 2018. 2018(1): p. 1-10.
86. Malathi, M. and P. Sinthia, *Brain tumour segmentation using convolutional neural network with tensor flow.* Asian Pacific journal of cancer prevention: APJCP, 2019. 20(7): p. 2095.
87. Islam, T., et al., *Detection of brain tumor by using ANN.* International Journal of Research in Advent Technology, 2014. 2(4): p. 279-282.
88. Amin, J., et al., *Detection of brain tumor based on features fusion and machine learning.* Journal of Ambient Intelligence and Humanized Computing, 2024. 15(1): p. 983-999.
89. Usman, K. and K. Rajpoot, *Brain tumor classification from multi-modality MRI using wavelets and machine learning.* Pattern Analysis and Applications, 2017. 20(3): p. 871-881.
90. Farhi, L., R. Zia, and Z.A. Ali, *Performance analysis of machine learning classifiers for brain tumor MR images.* Sir Syed University Research Journal of Engineering & Technology, 2018. 8(1): p. 6-6.

91. Afshar, P., A. Mohammadi, and K.N. Plataniotis, *Bayescap: A bayesian approach to brain tumor classification using capsule networks.* IEEE Signal Processing Letters, 2020. 27: p. 2024-2028.
92. Gumaei, A., et al., *A hybrid feature extraction method with regularized extreme learning machine for brain tumor classification.* IEEE Access, 2019. 7: p. 36266-36273.
93. Phaye, S.S.R., et al., *Dense and diverse capsule networks: Making the capsules learn better.* arXiv preprint arXiv:1805.04001, 2018.
94. Khan, Z., et al., *A comprehensive dataset of Infant Facial Expressions of Pain Intensity.* PeerJ Computer Science, 2026. 12: p. e2929.